

# Revealing CNN Architectures via Side-Channel Analysis in Dataflow-based Inference Accelerators

Hansika Weerasena, *Member, IEEE*, and Prabhat Mishra, *Fellow, IEEE*

**Abstract**—Convolution Neural Networks (CNNs) are widely used in various domains. Recent advances in dataflow-based CNN accelerators have enabled CNN inference in resource-constrained edge devices. These dataflow accelerators utilize inherent data reuse of convolution layers to process CNN models efficiently. Concealing the architecture of CNN models is critical for privacy and security. This paper evaluates memory-based side-channel information to recover CNN architectures from dataflow-based CNN inference accelerators. The proposed attack exploits spatial and temporal data reuse of the dataflow mapping on CNN accelerators and architectural hints to recover the structure of CNN models. Experimental results demonstrate that our proposed side-channel attack can recover the structures of popular CNN models, namely Lenet, Alexnet, and VGGnet16.

**Index Terms**—Neural network, CNN accelerator, side-channels.

## I. INTRODUCTION

Convolution Neural Networks (CNNs) [1] are Deep Neural Networks (DNNs) that incorporate convolution (Conv) layers specialized in processing multidimensional data. CNNs are used in a wide range of applications, such as image and video recognition, classification, and analysis. These neural networks operate in two main phases: training and inference. The training phase involves a time-consuming process of learning weights in the neural network, while inference uses the pre-trained neural network to perform fast predictions. Resource-constrained edge devices perform inference in the device rather than sending data to a centralized server for inference. These edge devices can range from mobile phones to remote offline sensor networks.

Edge artificial intelligence (AI) has the benefit of overcoming edge-to-server communication bottlenecks, high availability without depending on the internet, real-time insights, and reduced storage. AI at edge needs inference of pre-trained CNN models on resource-constrained devices with energy and area constraints. General-purpose central processing units (CPUs) or graphics processing units (GPUs) can be used for the purpose of training and inference of CNNs. Although central CPUs or GPUs are used in training these CNNs at servers, dataflow-based accelerators are preferred for inference at edge devices. Dataflow is a computing scheme that utilizes inherent data reuse of Conv layers to achieve efficient CNN inference performance. Dataflow-based CNN accelerators save energy and execution time by reducing the cost of main memory accesses by introducing a local memory hierarchy inside the accelerator [2]. Dataflows can be categorized into multiple taxonomies [2] depending on the data type that is kept stationary. This paper explores two widely used dataflows: weight-stationary (WS) and output-stationary (OS). These

dataflow accelerators can be designed using Application Specific Integrated Circuit (ASIC) as well as Field-Programmable Gate Array (FPGA). ASIC-based accelerators are preferred in edge inference since they are energy efficient while providing adequate computational flexibility.

These CNN models need to be run on various edge devices with diverse hardware, software, and firmware developed by different vendors. Supply chain vulnerability can lead to security concerns for these edge devices with accelerators. For example, hardware Trojans can be inserted during the design as well as fabrication phase of an ASIC-based accelerator with the malicious intent of leaking sensitive information without being detected at the post-silicon verification stage or during runtime [3]. In many application scenarios, the structure of a CNN model should be kept confidential for the following reasons. (1) CNN model can be a company's proprietary and critical intellectual property. (2) Knowing the network model leads to designing and launching efficient adversarial attacks [4]. (3) User privacy can be compromised in a shared accelerator if the model type is leaked. Different types of side-channel analysis (memory, timing, electromagnetic emanation) are used in recovering CNN structures from GPU/CPUs [5], [6], [7], [8], [9]. GPUs/CPUs use a temporal computing paradigm where centrally controlled processing units can only fetch data from the memory hierarchy. On the other hand, dataflow-based accelerators have a spatial computing paradigm where transfer between individually controlled processing units is possible. Due to the inherent difference in computing paradigm and underlying architecture, existing side-channel attacks on GPU/CPU-based accelerators cannot be directly applied to dataflow-based accelerators. Furthermore, existing memory-based side-channel attacks [10] on CNN processing focus on main memory to accelerator memory transfer, which leads to reverse-engineering a large set of possible CNN structures for a single CNN model. For example, [10] gives 24 possible structures for Alexnet [11].

In this paper, we try to answer a fundamental question: *is it possible for an adversary to exploit inherent data reuse of dataflow-based CNN inference accelerators via memory side-channels to accurately recover architectures of CNN models?* Our proposed research needs to answer two major challenges in developing such an attack: (1) how to exploit different dataflow patterns to converge a large number of potential structures to a few, although different layer structures can result in the same side-channel values, (2) how to develop a generalized approach to recover structures from different input, output, layer sizes and their mapping on the accelerator? CNN

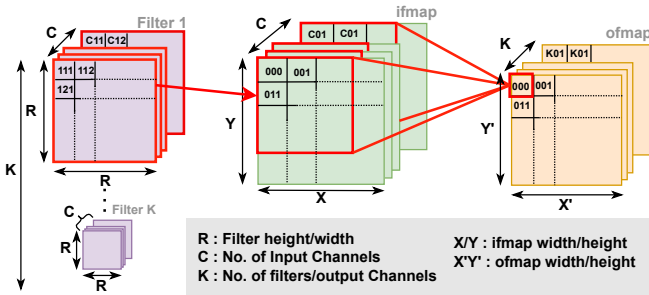


Fig. 1: Convolution layer parameters, semantics and operation: A  $R \times R \times C$  filter is applied on same size neighborhood of *ifmap* of size  $X \times Y \times C$  to calculate single value in *ofmap* of size  $X' \times Y' \times K$ .

consists of a sequence of Conv, fully-connected (FC), and pooling layers. Due to the prevalence of Conv layers and their inherent data reuse, CNN accelerators focus on accelerating convolution layers. Therefore, our study primarily focuses on extracting Conv layer structure while recovering the entire CNN architecture. Specifically, this paper makes the following important contributions.

- We define a threat model to gather memory-based side-channel information from a dataflow-based CNN inference accelerator.
- We propose a framework to recover the structure of Conv and FC layers from weight-stationary and output-stationary dataflow-based CNN inference accelerators with local forwarding.
- We propose a method to recover pooling layer parameters from a pooling module inside the CNN accelerator.
- Experimental results demonstrate that our approach can fully recover CNN architectures from popular CNN models (Lenet [12], Alexnet [11], VGG-16 [13]).

The rest of the paper is organized as follows. Section II presents background on CNN and dataflow-based accelerators. Section III outlines the threat model. Section IV describes our proposed approaches for extracting CNN architectures. Section V presents the experimental results. Finally, Section VI concludes the paper.

## II. BACKGROUND AND RELATED WORK

### A. Convolutional Neural Networks (CNN)

CNN mainly consists of three types of layers: convolutional, pooling, and fully-connected (FC) layers [1]. Convolution layers dominate the computations in CNN (about 90% [14]). A convolution layer takes an input activation/input feature map (*ifmap*) and does 2-D convolution using a set of filters with weights to obtain an output feature map (*ofmap*). Applying different filters results in extracting different embedded features from the *ifmap*. Figure 1 illustrates a typical convolution operation with  $K$  convolution filters of size  $R$  and having  $C$  input channels. It shows how the first element of *ofmap* is calculated by the sum of element-wise multiplication between a filter of size  $R \times R \times C$  and the same size neighborhood of

*ifmap*. Stride and padding are two other vital parameters of a convolution layer. Stride ( $St$ ) represents the number of values a filter moves horizontally or vertically during a convolution operation. Padding ( $Pd$ ) is the number of additional values around the edges of the *ifmap* before applying the convolution filter. All convolution layers follow the relationship in Equation 1. The same relationship holds for  $Y$  and  $Y'$ .

$$X' = ((X - R + 2Pd)/St) + 1 \quad (1)$$

In an FC layer, all the values of *ifmap* are connected to all the values of *ofmap*. In other words, a single *ofmap* value is composed using the weighted sum of all the *ifmap* values. The pooling layer is typically used after *conv* layer to reduce the dimensionality of the feature map. Max pooling and average pooling are two frequently used pooling operations [15]. Conv and FC layer execution can be viewed as a set of multiply and accumulate (MAC) operations, and modern accelerators perform a large number of MAC operations in parallel.

### B. Dataflow-based CNN Accelerators

Different highly-parallel computing paradigms are used in the processing of CNNs, namely temporal and spatial architectures [2]. CPUs/GPUs are categorized as temporal architectures, which have a large number of centrally controlled processing elements (PEs) with arithmetic and logic units. They can fetch data from the memory hierarchy but cannot communicate with each other. GPUs and CPUs use kernel-based accelerations by mapping FC and Conv layers to matrix operations. On the other hand, dataflow-based accelerators fall into spatial architectures where each PE has its own control logic and register. Dataflow-based accelerators use effective mapping of MAC operations to minimize main memory access, which results in low power and better execution time.

The CNN accelerators considered in this study process the CNN layer by layer [10]. In other words, the accelerator loads *ifmap*/weights of a particular layer to the global buffer, processes it, and writes *ofmap* of the layer back to the main memory. Dataflow determines how the data is moved and processed through the accelerator architecture to perform MAC operation needed for a CNN layer. Dataflow mapping refers to how MAC operations are assigned to each processing element in each cycle. Dataflow-based CNN accelerators try to get maximum data reuse efficient dataflow mapping. A typical architecture [16], [10] of a dataflow-based CNN inference accelerator used in edge devices is shown in Figure 4. The controller, interconnects, global buffer (GB), and PE arrays can be identified as critical components of a CNN accelerator.

A typical CNN accelerator supports three separate Network-on-Chip (NoC)/interconnects [17], [18] for two reasons: (1) different data types (weights/*ifmaps*/*ofmaps*) need different data transmission patterns (unicast, multicast, and broadcast), and (2) enables high-speed data transfer and pipelined operation. Dataflow defines how PEs and interconnects are arranged. There are weight-stationary (WS) [19], [20], [17] and output-stationary (OS) [21] dataflow based architectures with subtle differences. Our study focuses on the dataflow aspect of the

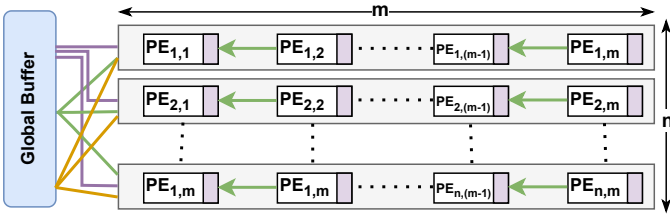


Fig. 2:  $WS(m, n)$  architecture: weight-stationary dataflow with  $n$  processing element (PE) arrays and  $m$  PEs per array, with separate interconnects for weight/input reads and partial sum reads and writes from/to Global Buffer (GB). Neighboring PEs in an array has input-forwarding connections.

accelerator by using a generic WS (section II-B1) and OS (section II-B2) dataflow architecture with input forwarding.

1) *Weight Stationary Dataflow*: As the name suggests, once a weight value is read to a PE, a WS dataflow does all the MAC operations involving that weight before reading a new value to a PE. Figure 2 shows an architecture of a weight-stationary dataflow that reuses weights temporarily and input activations spatially. It has  $n$  PE arrays, each with  $m$  PEs and denoted by the notation  $WS(m, n)$ . This accelerator has unicast NoC for weight, PE array-wise multicast supported NoC for inputs, another interconnect for partial sum reads, and a fixed accumulation tree NoC with adders similar to [17]. There are separate adder trees per array, and an adder tree will accumulate/sum up all weight activation products of an array in the preceding cycle. The resulting value is a partial sum (*psum*) for a one *ofmap* entry. This architecture can process multiple filters simultaneously using separate PE arrays per filter. This architecture minimizes *ifmap* reads by spatial reuse in two ways: (1) PE array-wise multicast shares the same input values across multiple PE arrays where each PE array calculates for a different filter, and (2) forwarding connection in a PE array can share activation values between two cycles occurring due to the stride of the filter. This weight-stationary architecture has flexibility in mapping, depending on the layer, the in-between forwarding connections between PEs can be switched on/off. Mapping of the layer to the PEs is optimized for maximum PE utilization and minimizing input reads. For example, if  $m = 4$  and  $n = 1$ , the first row of two channels of  $2 \times 2 \times 2$  CNN filter can be mapped as shown in Figure 3(a). If the filter size is  $4 \times 4 \times 2$ , only one channel row of the filter is mapped in the first cycle as shown in Figure 3(b). Both of the examples have a stride of one.

2) *Output Stationary Dataflow*: An output-stationary dataflow accumulates *psums* corresponding to one *ofmap* value in the internal register of a PE until it is fully calculated. In other words, a PE is mapped to a single value of *ofmap* until that value is fully calculated. Similar to the WS dataflow architecture discussed in Figure 2, it has  $n$  PE arrays, each with  $m$  PEs and denoted by the notation  $OS(m, n)$ , but with the following modifications. Instead of the internal register keeping weights stationary, it accumulates *psums*. This accelerator has unicast NoC for inputs, single value broadcast supported NoC

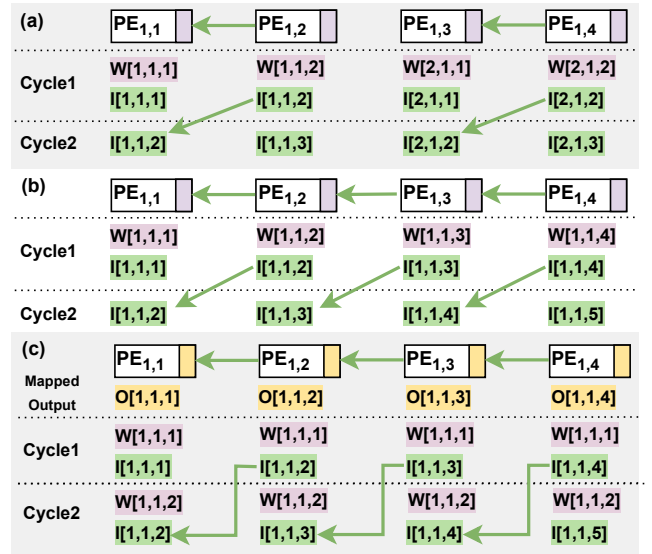


Fig. 3: Dataflow mapping and data reads for the first two cycles for three scenarios: (a) mapping of  $2 \times 2 \times 2$  filter into  $WS(4, 1)$ , (b) mapping of  $4 \times 4 \times 2$  filter into  $WS(4, 1)$ , and (c) mapping of  $2 \times 2$  filter into  $OS(4, 1)$  with  $st = 1$  and  $pd = 0$  and *ifmap* of  $\{X = 5, Y = 5, C = 2\}$ , and *ofmap* of  $\{X' = 4, Y' = 4, K = 1\}$ .

for weights, and separate interconnect to write outputs to the GB. One PE array will accumulate sums relevant to one row of *ofmap* so that forwarding links between PEs in the array can have maximum utilization. Due to the broadcast of a single weight, every PE calculates MAC relevant to one input channel in a cycle. In the first cycle, the accelerator multicasts the same weight to all the PEs and unicasts relevant activations to each PE. After doing MAC operations and accumulating the partial sum to the internal registry, different weight is broadcast in the second cycle. After the local forwarding of inputs, the remaining inputs are unicast relevant to the previous partial sum. Figure 3(c) shows a layer mapping with one filter with parameters  $\{R = 2, C = 2, st = 1, pd = 0\}$ , *ifmap* of  $\{X = 5, Y = 5, C = 2\}$ , and *ofmap* of  $\{X' = 4, Y' = 4, K = 1\}$  to a  $m = 4$  and  $n = 1$  output stationary accelerator. As we can see, there is only one input read ( $I[1,1,5]$ ) in the second cycle due to spatio-temporal forwarding of inputs ( $I[1,1,2]$  and  $I[1,1,3]$ ) from the previous cycle.

### C. Related Work

There are many efforts on leaking DNN/CNN architectures using side-channel attacks. Timing and memory side channels have been used to recover DNN models in [7], [10], [5], [6]. An attack to recover compact DNN models from GPU using timing, memory, power, and kernel side channels is proposed in [6]. They assume the attacker knows power consumption, memory footprint, and latency for backward and forward propagation for different batch sizes. Hu et al. [5] propose a method to find DNN architecture by eavesdropping into off-chip data transfer between CPU and GPU and exploiting the entire DNN execution stack (the DNN library, Hardware abstraction, and Hardware). Another side-channel attack on

analyzing main memory to accelerator memory access trace and execution time is discussed in [10]. The adversary can control the input to the accelerator and derive a set of potential models for the currently running DNN model. For example, they propose 24 possible structures for Alexnet. Wei et al. [7] exploit context switching of GPU to recover DNN models. This attack is made in the training stage because they can exploit multiple uses of the same layers over training time. Apart from memory and timing side channels, attacks are proposed on cache side channels to recover DNN models [8], [22], [23]. A few attacks can be seen using power [24] and electromagnetic side channels [9], [25] to recover CNN model structures. These studies validate that recovering DNN/CNN architecture is a critical security concern. To the best of our knowledge, our paper is the first study on recovering CNN model architecture using memory side channels of dataflow-based CNN inference accelerators.

### III. THREAT MODEL AND PROBLEM FORMULATION

Figure 4 illustrates an overview of a typical dataflow-based CNN accelerator with layer-by-layer execution described in section II-B. If we zoom into the processing of one layer, first, the host CPU loads *ifmap*/weights to the GB. These *ifmaps*/weights are stored as arrays in memory, which means they are stored in contiguous memory locations, and GB preserves the order. The PE arrays are designed in a pipelined manner to do MAC operations in each cycle. Each PE in the PE array has a local registry to hold or accumulate certain data elements to reuse in MAC operations. The controller is responsible for loading weights/inputs/*psums* to individual PEs in each cycle. The controller first calculates memory requests for the next cycle depending on the dataflow supported by the accelerator and layer parameters. Then, it issues memory requests to the global buffer. The global buffer uses interconnects between GB and PE arrays for data transfer.

The threat model assumes the adversary gathers the following memory side-channel information regarding the execution of each layer CNN: (1) the total number of weight/input reads and output writes, (2) the number of weight/input reads, output writes each cycle of execution until a *targeted event* ( $e$ ) that depends on the dataflow (the concrete definition of  $e$  in WS and OS dataflow are stated in section IV-C and IV-D respectively.), and (3) output stationary dataflow needs the virtual address of weight reads in the first two cycles. Here, an input read means reading of a single value from an *ifmap* and an output write means writing of a single value to an *ofmap*. Depending on the adversary’s capabilities, there are several ways to obtain these three pieces of information. The adversary can exploit unprotected communication between accelerator components. Information (1) and (2) can be obtained by snooping interconnects from GB to PE arrays (a in Figure 4). Since these accelerators use separate interconnects for each data type, it is easy to distinguish and count GB accesses that can be snooping on the interconnects. Alternatively, the adversary can obtain information (1) and (2) along with (3) by snooping the unprotected bus between the controller to

GB (b in Figure 4). If there is a pooling layer, for the recovery pooling layer parameters, the adversary needs to find the number of pooling operations ( $N_{pool}$ ).  $N_{pool}$  can be recovered using the number of output writes to DRAM from GB (c in Figure 4) during the layer execution. Snooping of these buses (a, b and c) can be done either through physical probing of buses or through a hardware Trojan. Alternatively, a compromised accelerator firmware or host operating system can steal relevant side-channel ((1), (2), and  $N_{pool}$ ) information by accessing performance counters.

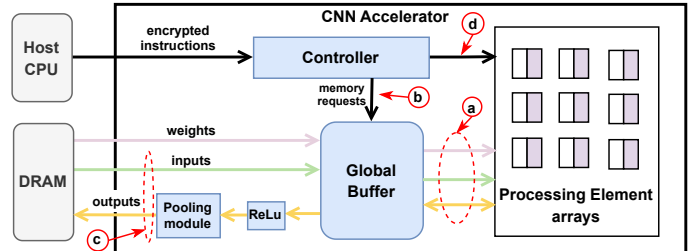


Fig. 4: Overview of a typical CNN accelerator. The controller, interconnects, global buffer (GB), and processing element (PE) arrays are the critical components. Unprotected communication can be snooped to extract side-channel data.

Our threat model also assumes that the adversary knows the accelerator architecture (number of PE arrays, number of PEs in an array, and the bandwidth of interconnects for each data type) as well as the dataflow mapping of each accelerator described in Section II-B. We also assume the adversary knows the *ifmap* parameters ( $X, Y, C$ ) of the first layer. In the layer-by-layer recovery of CNN, knowing the previous layer *ofmap* parameters can be directly used as *ifmap* parameters for the next layer. In other words, knowing the *ifmap* parameters of the first layer and recovering the parameters of that layer indirectly finds the *ifmap* parameters of the second layer. The proposed attack is passive, where the adversary can only snoop on the side-channel information but cannot alter dataflow mapping or data communication inside the accelerator. Furthermore, the adversary does not need to know the training or testing data of the CNN model.

### IV. EXTRACTING CNN ARCHITECTURE USING SIDE-CHANNEL ANALYSIS

Algorithm 1 shows an overview of the attack for recovering potential CNN structures from a dataflow-based accelerator. Lines 3-9 elaborate layer-by-layer side-channel data collection, which needs recognizing layer boundaries (line 5) discussed in Section IV-A. In each side-channel variable, the Superscript ( $j$  or  $k$ ) specifies the layer number relevant to the variable. Lines 10-14 elaborate layer-by-layer structure recovery. The first dimension of the *layers* 2D array (line 10) contains the number of layers ( $j$ ) in CNN, and the second dimension contains possible structures for each layer. In layer-wise structure recovery, as the first step, the layer type is identified (line 12), which is discussed in Section IV-B. Then the side-channel information is used to recover each layer’s parameters

(line 14). It is important to notice that if there are multiple potential structures for the previous layer, the algorithm tries *ifmap* parameters  $(X, Y, C)$  of all of them to recover potential structures for the current layer (loop at line 13). Finally, the adversary flatten the 2D array *layers* to multiple 1D arrays satisfying  $ifmap_j = ofmap_{j-1}$  to get all the potential structures of the CNN model (line 15).

Algorithm 2 zooms into recovering individual layer structures. Depending on the layer type, the layer recovery procedure calls different functions (line 3, 5 and 8). The most crucial and difficult task is to recover Conv layer. The subscript in *recoverConvDF* highlights that the recovery of the Conv layer depends on the dataflow. Therefore, recovery of Conv from WS dataflow and OS dataflow are elaborated in Section IV-C and IV-D, respectively. The function *recoverConvDF* returns a list of potential structures ( $H$ ) but the conditional filters used in recovering Conv layers in WS and OS dataflows ensure that  $H$  is a list with a few solutions or one solution (Section V shows Conv layer recovery in popular benchmarks converging to one structure). The recovery of FC (line3) and pooling (line 8) layers are discussed in Section IV-E and IV-F, respectively. Table I outlines the notations used in these algorithms. Figure 5 presents a high-level overview of our proposed side-channel attack.

---

#### Algorithm 1 Recovering potential CNN structures

---

```

1: Input: First ifmap parameters,  $\{X^1, Y^1, C^1\}$ 
2: Output: Potential CNN architectures
3:  $j = 1$  ▷ to count the number of layers
4: while processing of the CNN do
5:   while IdentifyLayerBoundary() do
6:      $W_r^j, I_r^j, O_w^j \leftarrow$  collect total R/W counts
7:      $w^j, i^j, o^j \leftarrow$  collect cycle-wise R/W counts until
       event  $e$ 
8:      $N_{pool}^j \leftarrow$  collect No. of pooling operations
9:      $j++$ 
10:  $layers = []$  ▷ empty 2D array
11: for  $k=1$  to  $j$  do
12:    $type \leftarrow$  IdentifyLayerType( $W_r^k, I_r^k, O_w^k, N_{pool}^k$ )
13:   for number of layer structures in  $layers[k-1]$  do
14:      $layers[k] \cup$  recoverLayer( $W_r^k, I_r^k, O_w^k, w^k, i^k, o^k, X^k, Y^k, C^k, type$ )
15: Return Flatten 2D array layers to multiple 1D arrays
       satisfying  $ifmap_j = ofmap_{j-1}$  to get all potential
       structures.

```

---

#### A. Identification of Layer Boundary

We present two ways to identify layer boundaries in a dataflow-based accelerator. The first method is to use the Read-After-Write (RAW) dependency of *ifmap* current layer and *ofmap* of the previous layer. Dataflow accelerators have sequential execution of the layers. Therefore, upon a successful layer execution, the *ofmap* is written back to the hosts' main memory (DRAM) and read it back to GB in the next layer as

---

#### Algorithm 2 Recovering layer parameters

---

```

1: function recoverLayer( $W_r, I_r, O_w, w, i, o, X, Y, C, type$ )
2:   if  $type = FC$  then
3:      $layer \leftarrow$  recoverFC( $W_r, I_r, O_w$ )
4:   if  $type = Conv$  then
5:      $H \leftarrow$  recoverConvDF( $W_r, O_w, w, i, o, X, Y, C$ )
6:     if Conv layer has pooling then
7:       for  $h$  in  $H$  do
8:          $h \cup$  recoverPooling( $N_{pool}, X', Y', K$ )
9:      $layer \leftarrow H$ 
10:  retrun  $layer$ 

```

---

TABLE I: Table of notations.

$n$	Number of PE arrays in an accelerator
$m$	Number of PEs per array in an accelerator
$W_r$	Total no. of weight reads for the layer execution.
$I_r$	Total no. of input reads for the layer execution.
$O_w$	Total no. of output reads for the layer execution.
$t_e$	Cycle number of the targeted event $e$ .
$w$	Array of no. of weight reads at each cycle.
$i$	Array of no. of input reads at each cycle.
$o$	Array of no. of output writes at each cycle.
$i[t]$	Number of input reads at $t^{th}$ cycle.
$w[t]$	Number of weight reads at $t^{th}$ cycle.
$\&(dt)$	Virtual address of data $dt$ in global buffer.
$H$	Possible parameter sets for a Conv Layer.
$ceil(x)$	Round-up number $x$ to nearest integer.

---

*ifmap*. This event can be identified using the memory trace as a RAW dependency on the same memory address. This needs an adversary needs to collect or actively observe the memory trace (address and cycle) between the GB and DRAM of the host. Similar to collecting previous side-channel information, this can be done by snooping the memory bus between GB to DRAM (© in Figure 4).

The second method is by identifying the configuration phase between layers. However, this approach is applicable in accelerators that have some reconfigurability. Since each layer differs, there is a configuration phase to dataflow mapping at each layer. Most CNN accelerators use a separate low-bandwidth bus (d in Figure 4) to send these configurations. Therefore, looking at active periods in that network is a simple way to identify boundaries. For example, the WS dataflow-based accelerator configures (on/off) forward links between PEs configured at each layer's beginning. The adversary can listen to this control message to identify layer boundaries.

#### B. Identification of Layer Type

The adversary needs to separate between FC, Conv, and Pooling layers. Because of no data reusability in FC layers, the total number of weight reads ( $W_r$ ) in a layer is equal to the multiplication between the total number of input reads ( $I_r$ ) and output writes ( $O_w$ ). This relationship is used to distinguish an FC layer from a Conv layer. If there is a pooling layer after the execution of Conv layer, CNN accelerators run the Conv layer together with the pooling layer using a separate pooling module as shown in Figure 4 (They are not processed as two

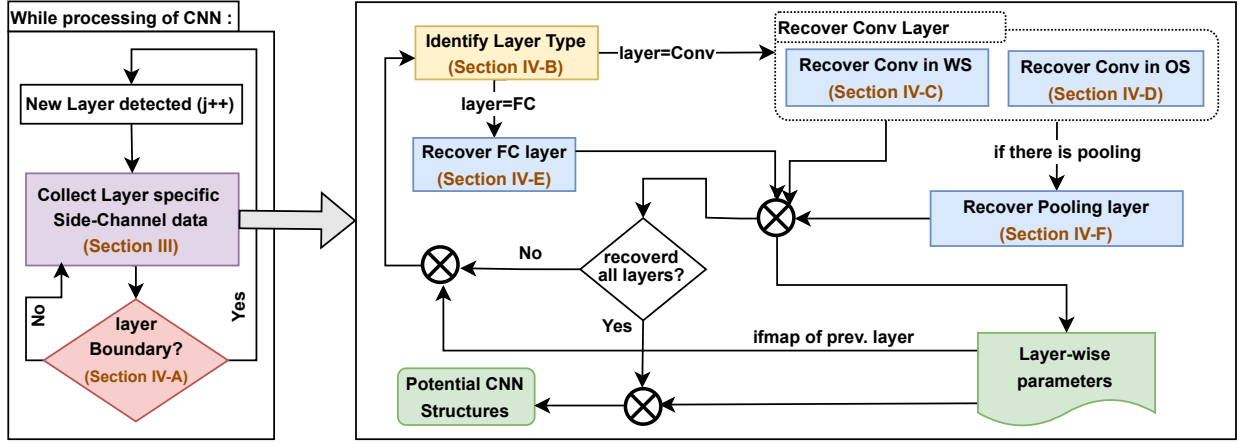


Fig. 5: Overview of the proposed side-channel attack to recover CNN model. The adversary collects layer-by-layer side-channel information, and utilizes them to recover layer-by-layer CNN structure.

separate layers). An adversary can detect a pooling layer by observing a difference between the number of outputs written to the global buffer and those written to DRAM inside the layer boundary.

### C. Recovery of Conv Layer from Weight-Stationary Dataflow

There are five parameters ( $R, C, K, St, Pd$ ) that define a Conv layer. Since the number of input channels ( $C$ ) is known from *ifmap* parameters, an adversary needs to find four parameters ( $R, K, St, Pd$ ) for successful Conv layer recovery. Algorithm 3 describes the attack steps for recovering a Conv layer from the WS dataflow based architecture outlined in Section II-B. We refer to the 1<sup>st</sup> cycle relative to each layer which is the first cycle with data transfer between GB to PE arrays. Here we define the *targeted event* for the cycle-to-cycle data collection as the cycle  $t_e$  where  $i[1] = i[t_e]$ . In other words, the adversary collects data reads/writes between the first cycle and the next ones with the same number of reads in the first cycle. This collects the number of data reads/writes accountable for the one row of the output feature map.

Due to the inherent feature of a WS dataflow, a single weight value is read only once:

$$W_r = R^2 \times C \times K \quad (2)$$

Solving of Equation 2 with known  $C$  in positive integer ( $\mathbb{Z}^+$ ) domain provides potential solutions ( $H$ ) for  $\{R, K\}$  values of the layer parameters (line 2). Then the adversary calculates  $n_a$ , the number of active PE arrays in the accelerator. Most of the time, the number of filters ( $K$ ) is greater than the number of PE arrays ( $n$ ) of the accelerator architecture, then  $n_a = n$ . Due to the *targeted event* of data collection, the number of cycles between reveals the width of the output feature map ( $X'$ ) (line 4). Even when  $R > m$  and folding is supported, the number of cycles up to the event minus one reflects the value of  $X'$ . Then the adversary iterates (lines 5 - 16) through the potential  $\{R, K\}$  values and uses architectural hints and side-channel information to filter out incompatible  $\{R, K\}$ . The first condition (line 6) applies when the potential

### Algorithm 3 Recovering Conv Layer from WS dataflow

```

1: function recoverConvws( $W_r, O_w, w, i, o, X, Y, C$ )
2:    $H \leftarrow$  solve Equation 2  $\in \mathbb{Z}^+$ 
3:    $n_a \leftarrow w[1]/i[1]$ 
4:    $X' \leftarrow t_e - 1$ 
5:   for  $\{R, K\}$  in  $H$  do
6:     if  $R \leq w[1]/n_a$  and  $(w[1]/n_a)\%R \neq 0$  then
7:       remove  $\{R, K\}$ 
8:      $st \leftarrow i[2]/\max((m//R), 1)$ 
9:     if  $st \notin \mathbb{Z}^+$  or  $st > R$  then
10:      remove  $\{R, K\}$ 
11:      $pd \leftarrow$  substitute  $\{R, st\}$  and  $X, X'$  to Equation 1
12:     if  $pd \notin \mathbb{Z}^+$  or  $pd > R$  then
13:       remove  $\{R, K, st\}$ 
14:      $Y' \leftarrow$  substitute  $\{R, st\}$  and  $Y, pd$  to Equation 1
15:     if  $O_w \neq X' \times Y' \times K$  then
16:       remove  $\{R, K, st, pd\}$ 
17:   return  $H$ 

```

value of  $R$  is smaller than the active PE array length ( $w[1]/n_a$ ). As discussed in Section II-B, the adversary uses the dataflow-mapping property of the accelerator to minimize input reads by only fully mapping filter rows. For example, if the PE array length is 12 ( $m = 12$ ) and  $R, K$  are 5 and 4, the layer is mapped as two 10 MACs across two channels by utilizing only 10 PEs, not 12 Macs followed by 8. Line 6 checks the condition  $((w[1]/n_a)\%R \neq 0)$  and filter out solutions.

The adversary calculates the stride ( $st$ ) of the respective potential  $R$  (line 8). Since the forward links between PEs are used to forward *ifmap* values from the previous cycle, the number of new input reads for the current cycle is always an integer multiple of stride. At line 8,  $m//R$  ( $//$  is the integer division) gives out the number of channels of a filter mapped to the PE array when  $m \geq R$ . If  $m < R$  and folding is used, only one channel is mapped to a PE array. Taking the maximum, consider both conditions ( $m \geq R$  and  $m < R$

). The second cycle has input forwarding, and  $i[2]$  is the number of new input reads after input forwarding. Therefore, dividing  $i[2]$  by the number of channels mapped to one PE array is the stride for the selected  $R$ . The condition at line 9 checks if the previously calculated  $st$  is in the integer domain and is less than the filter size ( $R$ ). Then adversary can use Equation 1 to calculate  $pd$  and check if  $pd$  is in the integer domain and it is less than filter width ( $R$ ). Line 14 calculates  $Y'$  using the Equation 1 from previously found values ( $R, Y, st, pd$ ). The final condition asserts whether the side-channel information  $O_w$  equals expected output writes ( $X' \times Y' \times K$ ). The returned  $H$  has potential solutions for the layer's parameters  $\{R, K, C, st, pd\}$ . In WS dataflow,  $O_w$  is equal to the difference between the number of partial sum reads and writes ( $psum_w - psum_r$ ). The section V-C provides a case study on the second Conv layer of Alexnet, which converges into one solution.

#### D. Recovery of Conv Layer from Output-Stationary Dataflow

Algorithm 4 outlines the attack steps for recovering Conv layer parameters from the OS dataflow-supported architecture described in the Section II-B. Here we define the *targeted event* for the cycle-to-cycle data collection as the cycle where the first *ofmap* value is written. In other words, the adversary collects the cycle-to-cycle data from the first cycle to the cycle where the first *output* is written. In an OS dataflow, there are no partial outputs/sums. In other words, an *ofmap* value is written only after it is fully calculated. The intuition behind the *targeted event* selection is to find the number of weight reads responsible for fully calculating one *ofmap* value.

---

#### Algorithm 4 Recovering Conv Layer from OS dataflow

---

```

1: function recoverConvos( $W_r, O_w, w, i, o, X, Y, C$ )
2:    $eq \leftarrow R^2C = t_e - 1$ 
3:    $R \leftarrow \text{solve } eq \text{ for } R \text{ in } \mathbb{Z}^+$ 
4:    $st \leftarrow \&[w_1] - \&[w_2]$ 
5:   for  $pd = 0$  to  $R - 1$  do
6:      $X' \leftarrow$  substitute  $R, st, pd, X$  for Equation 1
7:      $Y' \leftarrow$  substitute  $R, st, pd, Y$  for Equation 1
8:     if  $X', Y' \notin \mathbb{Z}^+$  then
9:       continue ▷ Not a solution
10:     $K \leftarrow$  substitute  $\{X', Y'\}$  to Equation 3
11:    if  $K \in \mathbb{Z}^+$  and  $\{X', Y', R, K, C\}$  satisfy Eq. 4
12:  then
13:     $H \leftarrow H \cup \{R, K, C, st, pd\}$ 
14:  return  $H$ 

```

---

When we consider one *ofmap* value, it is generated from an accumulation of multiplications between a single filter of width and height of  $R$  with  $C$  channels. In other words, the total responsible weight reads for a single value in *ifmap* is  $R^2C$ . Our selection of the *targeted event* ensures that the  $(t_e - 1)$  equals  $R^2C$  (line 2). Since the architecture reads one weight in a cycle, the relationship in line 2 holds. Solving this relationship in the  $\mathbb{Z}^+$  domain gives the value of  $R$ . Because of the forwarding connections at each PE in the PE array, the

difference between the virtual address of weight reads from the controller gives the value of stride (line 4). Lines 5 to 11 iterate through all possible  $pd$  values. This loop termination considers that padding cannot exceed the filter width ( $R$ ). Lines 6 and 7 calculate the width ( $X'$ ) and height ( $Y'$ ) of the *ofmap* for the selected  $pd$ . The condition at line 8 checks if the calculated  $X', Y'$  is in  $\mathbb{Z}^+$  domain; if not, we move to the next  $pd$  value in the loop. In an OS dataflow, the number of total output written ( $O_w$ ) to the GB:

$$O_w = X' \times Y' \times K \quad (3)$$

Line 9 substitutes previously calculated  $\{X', Y'\}$  to the above equation and finds  $K$ . Line 9 checks for two conditions: (1) whether  $K$  is in  $\mathbb{Z}^+$  domain, and (2) does the relationship stated in Equation 4 holds for the potential value set  $\{X', Y', R, K, C\}$ ?

$$W_r = (\text{ceil}(\frac{X'}{m}) \times \text{ceil}(\frac{Y'}{n}))R^2CK \quad (4)$$

All PEs in this OS architecture conducts MAC operations relevant to one output channel due to the broadcasting of weights. Therefore, the *psum* accumulated at each registry is also relevant to a single output channel. When we zoom into Equation 4,  $(\text{ceil}(\frac{X'}{m}) \times \text{ceil}(\frac{Y'}{n}))$  gives the number of tiles needed to calculate all *ofmap* values of a single output channel. For example, if we process a layer with  $(X', Y' = 12, K = 1)$  in an  $OS(12, 4)$  architecture. The first tile calculates *ofmap* values for the first four rows and the second and third tiles for the middle four rows and last four rows, respectively. From the first line of the algorithm,  $R^2C$  gives weight reads for one tile. So, the number of tiles per single output channel  $\times$  weight reads per tile  $\times$  number of output channels gives the total weight reads. Section V-D shows a case study on the second Conv layer of Alexnet that converged into one solution.

#### E. Extraction of FC Layer Parameters

An FC layer can be considered a Conv layer with a filter size equal to the size of the input, effectively connecting all neurons to each other. Therefore, extracting FC layer parameters is relatively straightforward compared to extracting Conv layer parameters. An FC layer has only two parameters, which are input neuron size and output neuron size. FC layer parameters can be found independent of dataflow and underneath accelerator architecture by only looking at total data reads and writes for the layer. The total number of input reads in a layer ( $I_r$ ) equals the number of input neurons in an FC layer. Similarly, the total number of output writes ( $O_w$ ) equals the number of output neurons. Additionally, a dense FC layer has  $W_r = I_r \times O_w$  relationship.

#### F. Extraction of Pooling Layer Parameters

Our methodology to extract pooling layers from max or average pooling depends on three assumptions based on typical pooling operations on CNNs. (1) Usually, the stride is greater than 1 [2]. (2) Max and average pooling typically does not use padding. (3) CNNs tend to use small pooling filter

sizes because large pooling filters tend to overfit models by losing information. The pooling operation does not change the number of output channels ( $K$ ). Algorithm 5 outlines the steps to recover pooling layer parameters ( $\{R_{pool}, st_{pool}\}$ ) from side-channel information.

---

**Algorithm 5** Recovering pooling layer

---

```

1: function recoverPooling( $N_{pool}, X', Y', K$ )
2:   for  $R_{pool} = 2$  to  $X'$  do
3:     for  $st_{pool} = R_{pool}$  to 1 do
4:        $X_{pool} \leftarrow ((X' - R_{pool}) / st_{pool} + 1)$ 
5:        $Y_{pool} \leftarrow ((Y' - R_{pool}) / st_{pool} + 1)$ 
6:       if  $N_{pool} / K = X_{pool} \times Y_{pool}$  then
7:         return  $\{R_{pool}, st_{pool}\}$ 

```

---

The loop at line 2 searches for pooling layers for increasing filter sizes, which gives more dominance to small pool layers. The second loop (line 3) ensures the attack first tries to match a non-overlapping pooling layer and increases the overlapping in subsequent iterations. Line 4 and 5 calculates the *ofmap* width ( $X_{pool}$ ) and height ( $Y_{pool}$ ) after pooling. Finally, the condition at line 6 checks if the monitored  $N_{pool}$  satisfies the calculated  $\{X_{pool}, Y_{pool}\}$  values to find the pooling layer parameters.

## V. EXPERIMENTS

### A. Experimental Setup

We performed modifications on top of the cycle-accurate Stonne [26] accelerator simulator to model the WS dataflow described in Section II-B1 and an in-house cycle-accurate simulator to model the OS dataflow described in Section II-B2. We gathered the side-channel information using the global buffer of the simulator. We provide adequate bandwidth for interconnects of each data type (input, output, weight) in each simulation so that any data loads will happen in one cycle. We model a simple pooling module in both accelerators to mimic pooling operations and extract the number of pooling operations. We model three concrete weight-stationary accelerator architectures from the architecture described in Section II-B:  $WS(4, 4)$ ,  $WS(12, 4)$ , and  $WS(24, 10)$ . Similarly, we use three output stationary dataflow accelerators:  $OS(4, 4)$ ,  $OS(10, 4)$ , and  $OS(20, 10)$ . We attacked and recovered popular CNN models: a 5-layer Lenet, an 8-layer AlexNet, and a 16-layer VGGnet-16 to evaluate the proposed CNN model recovery attack. Table II shows an overview of our experimental setup.

### B. Results

As shown in Table II, we can fully recover CNN parameters for Lenet, Alexnet, and VGGnet-16 for both WS and OS dataflow accelerators of two sizes. The layer boundaries of WS dataflow are identified by monitoring the configuration phase and OS dataflow by observing RAW dependency of feature maps. The CNN structure has converged into one solution, which highlights that for each Conv layers Algorithm 3 and 4 converged to one solution ( $size(H) = 1$ ) for the respective layer parameters. This is because our method can recover exact

TABLE II: Number of potential structures recovered from Lenet, Alexnet, and VGGnet-16 using our method and comparison with [10] that exploit DRAM to GB memory access.

CNN model		Lenet	Alexnet	VGGnet-16
Number of layers (Conv/Pool/FC)		3/2/2	5/3/3	13/5/3
Conv layer filter sizes		5x5 2x2	11x11 5x5, 3x3	1x1 3x3
Number of potential structures	WS(4,4)	1	1	1
	WS(12,4)	1	1	1
	WS(24,10)	1	1	1
	OS(4,4)	1	1	1
	OS(10,4)	1	1	1
	OS(20,10)	1	1	1
[10]		9	24	-

values for some parameters ( $X'$  in WS and  $R$  and  $st$  in OS) and use them with multiple condition checks to converge to the potential structure.

TABLE III: Side channel data ( $I_r, O_w, W_r$ ) for all fully connected layers of Alexnet on OS and WS dataflows.

Layer	FC1	FC2	FC3
Input reads	9216	4096	4096
Weight reads	37748736	16777216	4096000
Output writes	4096	4096	1000

Since no approaches exist on dataflow architectures to recover CNN models, we compare our results with [10], which uses the DRAM to GB memory access patterns and execution time of layers on an FPGA-based accelerator to recover CNN models. They were able to recover six potential structures for Lenet and 24 potential structures for Alexnet. Since our approach exploits inherent dataflow patterns and data reuse that leak critical characteristics of layers, our solution converged into one correct structure in both cases across all architectures. Table III and IV shows side-channel data on all FC and pooling layers of Alexnet. The side-channel data of FC and pooling layers do not depend on the specific dataflow architecture of the accelerator. Section V-C and V-D provide two case studies using Alexnet to provide insight into the recovery procedure of Conv layers.

TABLE IV: Side channel data ( $N_{pool}$ ) for all pooling layers of Alexnet running on the pooling module.

Layer	Pool 1	Pool 2	Pool 3
Number of pool op.	69984	43264	9216

### C. Case Study: Alexnet with Weight-Stationary Dataflow

Table V shows the side-channel information used to recover all five Conv layers of Alexnet in the  $WS(12, 4)$  accelerator. The attack needs only a relatively small number of cycle-wise data to be collected. For example, the *targeted event* cycle in the second Conv layer is 55, while the total is 2395801 cycles. The rest of the section zooms in on recovering the second Conv layer of Alexnet using Algorithm 3.

The second Conv layer of Alexnet has 256 filters ( $K = 256$ ) with parameters  $\{R = 5, C = 96, st = 1, pd = 2\}$ . This layer

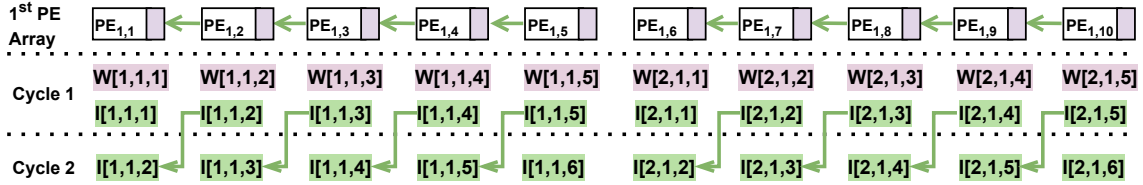


Fig. 6: Dataflow mapping at 1<sup>st</sup> and 2<sup>nd</sup> cycle of Alexnet Conv2 layer in WS(12,4) accelerator (only 1<sup>st</sup> PE array is shown).

TABLE V: Side-channel information for all five Conv layers on Alexnet running on WS(12, 4) and the number of cycles.

Layer	Weight reads	$psum$ reads	$psum$ writes	Event cycle	Total cycles
Conv1	614400	44603136	44789760	27	11197441
Conv2	34848	9292800	9583200	55	2395801
Conv3	884736	12395136	12460032	13	3115009
Conv4	1327104	18625152	18690048	13	4672513
Conv5	884736	12416768	12460032	13	3115009

takes a input feature map of size  $\{X = 27, Y = 27, C = 96\}$  and output a feature map of parameters  $\{X' = 27, Y' = 27, K = 256\}$ . According to the dataflow mapping described in Section II-B, this layer is mapped as two rows (row size = 5) of filter representing two input channels in one PE array. There are four such PE arrays representing different filters. Figure 6 shows the mapping of dataflow in the first two cycles in the first PE array with ten active PEs (the diagram does not show unmapped and idle PE(1,11) and PE(1,12)). The mapping of weights maximizes the input forwarding between two consecutive cycles (there are only two new input reads and eight forwarding in second cycle). The other three PE arrays load weights of filter 2-4 in the same relative order and use the same  $ifmap$  values provided to the first PE array through array-wise multicast.



Fig. 7: Cycle-wise number of data reads/writes until the targeted event of Alexnet Conv2 layer in WS(12,4).

Execution of the Conv2 of Alexnet in WS(12, 4) results in  $W_r = 34848$ ,  $psum_r = 9292800$ , and  $psum_w = 9583200$ . The rest of the section goes through the Algorithm 3 to recover Conv2 parameters of Alexnet. Figure 7 shows the cycle-by-cycle number of GB reads/writes of different data types. The set H with potential (R,K) values =  $\{(2,1600), (4,400), (5,256), (8,100), (10,64), (16,25), (20,16), (40,4), (80,1)\}$ . Then the number of active PE arrays can be calculated as  $n_a = 40/10 = 4$ . Since the targeted event occurs in the 27<sup>th</sup> cycle,  $X'$  is 27. Then let's look at each condition and what potential values are filtered out. The first condition (line 6) applies to the first five elements of H where  $R \leq 10$ . From these five values, (4,400)

and (8,100) are filtered out from H. For example  $(w^1/n_a)\%R$  is  $10\%4 = 2$  for (4,400).

When considering the next two conditions in lines 9 and 12, Table VI shows  $st$  and  $pd$  values generated according to the algorithm.  $i[2] = 2$  is from side channels, which is used to calculate  $st$  for each value remaining in set H. When we look at the table, only (5,256) satisfy both conditions. It is important to notice that potential  $R \geq 10$  fails the  $pd > R$  condition. When we consider the final condition and the remaining value of set H (5,256):  $X' \times Y' \times K = 186624$ , which is equal to  $O_w = psum_w - psum_r$ . Therefore, we can successfully recover Alexnets' Conv2 layer parameters.

TABLE VI: Checking conditions 2 and 3 of Algorithm 3 for Conv2 of Alexnet on WS(12, 4) dataflow accelerator.

(R,K)	(2,1600)	(5,256)	(10,64)	(16,25)	(20,16)	(40,4)	(80,1)
max(m/R,1)	6	2	1	1	1	1	1
st	4/6	1	2	2	2	2	2
pd	-	2	35/2	41/2	45/2	65/2	105/2
$x/\checkmark$	x	$\checkmark$	x	x	x	x	x

#### D. Case Study: Alexnet with Output-Stationary Dataflow

Table VII shows the side-channel information used to recover all the five convolution layers of Alexnet in the OS(10, 4) accelerator. The attack needs only a small number of cycle-wise data to be collected. For example, the targeted event cycle in the second Conv layer is 363, while the total is 2927233 cycles. The remainder of the section describes how to recover the second Conv layer of Alexnet using Algorithm 4.

TABLE VII: Side-channel information for all Conv layers on Alexnet running on OS(10, 4)

Layer	Weight reads	Output writes	Event cycle	Total cycles
Conv1	2927232	290400	363	2927233
Conv2	12902400	186624	2400	12902401
Conv3	7077888	64896	2304	7077889
Conv4	10616832	64896	3456	10616833
Conv5	7077888	43264	3456	7077889

The first Conv layer of Alexnet has 96 filters ( $K = 96$ ) with parameters  $\{R = 11, C = 3, st = 4, pd = 0\}$ . This layer takes an input feature map of size  $\{X = 227, Y = 227, C = 3\}$  and outputs a feature map of parameters  $\{X' = 55, Y' = 55, K = 96\}$ . Figure 8 shows dataflow mapping in the first two cycles: the first ten entries of the first row of the  $ofmap$  are accumulated in the first row of the PE array. Similarly, the subsequent three rows of the  $ofmap$  are mapped into the next three PE arrays in order. The weight reads in consecutive cycles are done to maximize input forwarding. For example, the reading of the  $W[1, 1, 5]$  in the second cycle

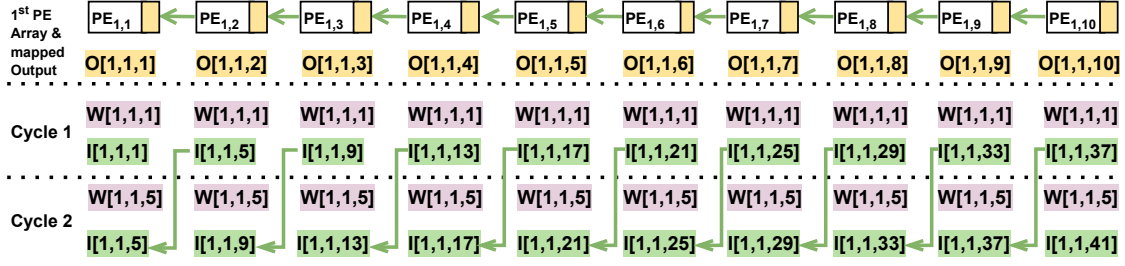


Fig. 8: Dataflow mapping at 1<sup>st</sup> and 2<sup>nd</sup> cycle of Alexnet Conv1 layer in  $OS(10, 4)$  accelerator (only 1<sup>st</sup> PE array is shown).

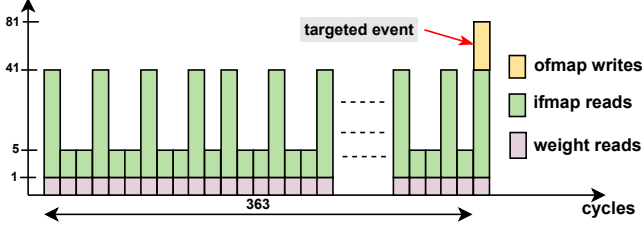


Fig. 9: Cycle-wise number of data reads/writes until the *targeted event* of Alexnet Conv1 layer in  $OS(10,4)$ .

after  $W[1, 1, 1]$  in the first cycle results in only one input read from GB ( $I[1, 1, 41]$ ) for that PE array. Only four input reads from GB in the second cycle for all four PE arrays.

Execution of the Conv1 of Alexnet in  $OS(10, 4)$  results in  $W_r = 2927232$  and  $O_w = 290400$ . The rest of the section goes through the Algorithm 4 to recover Conv1 parameters of Alexnet. Figure 9 shows the cycle-by-cycle number of GB reads/writes of different data types. The cycle of the *targeted event* ( $t_e$ ) is 364. Therefore,  $R^2C = 363$  (line 1). Solving this in the  $\mathbb{Z}^+$  domain gives  $R = 11$ . The virtual address difference between weight reads in the first ( $W[1,1,5]$ ) and second ( $W[1,1,1]$ ) cycle is 4, which is equal to the stride. When we consider the two conditions in lines 8 and 10, Table VIII shows  $X'/Y'$  and  $K$  values generated according to the algorithm for each potential  $pd$  value (0-10). As shown in the table, only  $pd = 0$  passes all the conditions.  $pd = 0$  also satisfies Equation 4 ( $2927232 = (\text{ceil}(55/10) \times \text{ceil}(55/4))11^2 \times 3 \times 96$ ). Therefore, we can successfully recover Alexnets' Conv1 layer parameters.

TABLE VIII: Checking conditions 1 and 2 of Algorithm 4 for Conv1 of Alexnet on  $OS(10, 4)$  dataflow accelerator.

pd	0	1	2	3	4	5	6	7	8	9	10
$X'/Y'$	55	55.5	56	56.5	57	57.5	58	58.5	59	59.5	60
$K$	96	-	92.6	-	89.3	-	86.3	-	83.4	-	80.6
$x/\checkmark$	$\checkmark$	x	x	x	x	x	x	x	x	x	x

### E. Applicability and Limitations

Our proposed attack works on any concrete configuration of abstract WS and OS dataflow architectures outlined in Section II. For this study, we assumed there is no bandwidth limitation on interconnect for each datatype. After relaxing this assumption, a minor modification in Algorithm 3 in WS dataflow or 4 in OS dataflow can generate the same results. For example, if weight NoC has a bandwidth limitation of 10 on the processing of the Conv layer in  $WS(12, 4)$ , as elaborated

in Figure 7, four cycles would be spent on the initial weight memory read. We can identify the initial four memory reads by either lagging of *psum* writes by three cycles or idling input interconnect for three cycles. Another assumption we made was the accumulation of multiplication on one PE array in WS dataflow happens in one cycle. If we relax this assumption and set  $q$  cycles for accumulating a *psum* write in a PE array, every *psum* write will lag by extra  $q-1$  cycles. A minor modification of calculating the event cycle as  $t_e - q$  can fix this. Our approach can be applied to folding-supported WS architectures since our attack uses side-channel information independent of folding. Our attack on WS dataflow can be extended to any WS accelerator with input forwarding as MAERI [17]. Our attack on OS dataflow can be extended to other OS architectures with input forwarding [21], [27] to recover CNN models.

In this paper, we develop a methodology for recovering CNN models from weight-stationary and output-stationary dataflow architectures with input forwarding. The underlying abstract methodology can be extended to recover CNN models from other dataflow architectures using different local forwarding data-type (e.g., Neuflow [28]) and different dataflow taxonomies (input-stationary and row stationary [29]) by (1) defining a *targeted event/events* to collect cycle-wise number of data reads and writes, (2) collecting total reads and writes responsible for a layer, and (3) exploiting spatial and temporal data reuse in (1) and (2) with architectural details. Our approach cannot be directly applied to recover CNN structures with sparse FC and Conv layers such as Squeezenet [30]. Our study on recovering CNN architectures highlights that memory access patterns should not be exposed to adversaries to avoid the leaking of CNN model architectures through dataflow-based CNN accelerators.

## VI. CONCLUSION

Artificial intelligence at edge devices is becoming increasingly ubiquitous with the abundance of data. Convolution neural networks (CNN) are executed using dataflow-based CNN accelerators due to energy efficiency. These accelerators use dataflows coupled with architectural designs to maximize different types of data reuse in CNN layers to efficiently perform inference using CNN models. This paper proposes an end-to-end memory-based side-channel attack that exploits dataflow patterns with the help of architectural hints to recover CNN model structures. Extensive evaluation of multiple architectures on weight stationary and output stationary dataflows

demonstrates that our proposed method can fully recover well-known benchmark CNN models running in these CNN accelerators. This work also highlights the importance of concealing memory access patterns in dataflow-based inference accelerators.

#### ACKNOWLEDGMENTS

This work was partially supported by National Science Foundation (NSF) grant SaTC-1936040.

#### REFERENCES

- [1] J. Gu, Z. Wang, J. Kuen, L. Ma, A. Shahroudy, B. Shuai, T. Liu, X. Wang, G. Wang, J. Cai *et al.*, “Recent advances in convolutional neural networks,” *Pattern recognition*, vol. 77, pp. 354–377, 2018.
- [2] V. Sze, Y.-H. Chen, T.-J. Yang, and J. S. Emer, “Efficient processing of deep neural networks: A tutorial and survey,” *Proceedings of the IEEE*, vol. 105, no. 12, pp. 2295–2329, 2017.
- [3] P. Mishra, S. Bhunia, and M. Tehranipoor, *Hardware IP security and trust*. Springer, 2017.
- [4] A. Chakraborty, M. Alam, V. Dey, A. Chattopadhyay, and D. Mukhopadhyay, “Adversarial attacks and defences: A survey,” *arXiv preprint arXiv:1810.00069*, 2018.
- [5] X. Hu, L. Liang, L. Deng, S. Li, X. Xie, Y. Ji, Y. Ding, C. Liu, T. Sherwood, and Y. Xie, “Neural network model extraction attacks in edge devices by hearing architectural hints,” *arXiv preprint arXiv:1903.03916*, 2019.
- [6] N. K. Jha, S. Mittal, B. Kumar, and G. Mattela, “Deeppeep: Exploiting design ramifications to decipher the architecture of compact dnns,” *ACM Journal on Emerging Technologies in Computing Systems (JETC)*, vol. 17, no. 1, pp. 1–25, 2020.
- [7] J. Wei, Y. Zhang, Z. Zhou, Z. Li, and M. A. Al Faruque, “Leaky dnn: Stealing deep-learning model secret with gpu context-switching side-channel,” in *2020 50th Annual IEEE/IFIP International Conference on Dependable Systems and Networks (DSN)*. IEEE, 2020, pp. 125–137.
- [8] M. Isakov, L. Bu, H. Cheng, and M. A. Kinsy, “Preventing neural network model exfiltration in machine learning hardware accelerators,” in *2018 Asian Hardware Oriented Security and Trust Symposium (Asian-HOST)*. IEEE, 2018, pp. 62–67.
- [9] H. Yu, H. Ma, K. Yang, Y. Zhao, and Y. Jin, “Deepem: Deep neural networks model recovery through em side-channel information leakage,” in *2020 IEEE International Symposium on Hardware Oriented Security and Trust (HOST)*. IEEE, 2020, pp. 209–218.
- [10] W. Hua, Z. Zhang, and G. E. Suh, “Reverse engineering convolutional neural networks through side-channel information leaks,” in *2018 55th ACM/ESDA/IEEE Design Automation Conference (DAC)*. IEEE, 2018, pp. 1–6.
- [11] A. Krizhevsky, I. Sutskever, and G. E. Hinton, “Imagenet classification with deep convolutional neural networks,” *Communications of the ACM*, vol. 60, no. 6, pp. 84–90, 2017.
- [12] Y. Le Cun, L. D. Jackel, B. Boser, J. S. Denker, H. P. Graf, I. Guyon, D. Henderson, R. E. Howard, and W. Hubbard, “Handwritten digit recognition: Applications of neural network chips and automatic learning,” *IEEE Communications Magazine*, vol. 27, no. 11, pp. 41–46, 1989.
- [13] K. Simonyan and A. Zisserman, “Very deep convolutional networks for large-scale image recognition,” *arXiv preprint arXiv:1409.1556*, 2014.
- [14] J. Cong and B. Xiao, “Minimizing computation in convolutional neural networks,” in *Artificial Neural Networks and Machine Learning—ICANN 2014: 24th International Conference on Artificial Neural Networks, Hamburg, Germany, September 15-19, 2014. Proceedings 24*. Springer, 2014, pp. 281–290.
- [15] I. Goodfellow, Y. Bengio, and A. Courville, *Deep learning*. MIT press, 2016.
- [16] R. Machupalli, M. Hossain, and M. Mandal, “Review of asic accelerators for deep neural network,” *Microprocessors and Microsystems*, vol. 89, p. 104441, 2022.
- [17] H. Kwon, A. Samajdar, and T. Krishna, “Maeri: Enabling flexible dataflow mapping over dnn accelerators via reconfigurable interconnects,” *ACM SIGPLAN Notices*, vol. 53, no. 2, pp. 461–475, 2018.
- [18] Y.-H. Chen, T.-J. Yang, J. Emer, and V. Sze, “Eyeriss v2: A flexible accelerator for emerging deep neural networks on mobile devices,” *IEEE Journal on Emerging and Selected Topics in Circuits and Systems*, vol. 9, no. 2, pp. 292–308, 2019.
- [19] V. Gokhale, J. Jin, A. Dundar, B. Martini, and E. Culurciello, “A 240 g-ops/s mobile coprocessor for deep neural networks,” in *Proceedings of the IEEE conference on computer vision and pattern recognition workshops*, 2014, pp. 682–687.
- [20] S. Chakradhar, M. Sankaradas, V. Jakkula, and S. Cadambi, “A dynamically configurable coprocessor for convolutional neural networks,” in *Proceedings of the 37th annual international symposium on Computer architecture*, 2010, pp. 247–257.
- [21] Z. Du, R. Fasthuber, T. Chen, P. Ienne, L. Li, T. Luo, X. Feng, Y. Chen, and O. Temam, “Shidiannao: Shifting vision processing closer to the sensor,” in *Proceedings of the 42nd Annual International Symposium on Computer Architecture*, 2015, pp. 92–104.
- [22] M. Yan, C. Fletcher, and J. Torrellas, “Cache telepathy: Leveraging shared resource attacks to learn dnn architectures,” in *USENIX Security Symposium*, 2020.
- [23] Y. Liu and A. Srivastava, “Ganred: Gan-based reverse engineering of dnns via cache side-channel,” in *Proceedings of the 2020 ACM SIGSAC Conference on Cloud Computing Security Workshop*, 2020, pp. 41–52.
- [24] Y. Xiang, Z. Chen, Z. Chen, Z. Fang, H. Hao, J. Chen, Y. Liu, Z. Wu, Q. Xuan, and X. Yang, “Open dnn box by power side-channel attack,” *IEEE Transactions on Circuits and Systems II: Express Briefs*, vol. 67, no. 11, pp. 2717–2721, 2020.
- [25] L. Batina, S. Bhasin, D. Jap, and S. Picek, “Csi nn: Reverse engineering of neural network architectures through electromagnetic side channel,” 2019.
- [26] F. Muñoz-Martínez, J. L. Abellán, M. E. Acacio, and T. Krishna, “Stonne: Enabling cycle-level microarchitectural simulation for dnn inference accelerators,” in *2021 IEEE International Symposium on Workload Characterization (IISWC)*. IEEE, 2021, pp. 201–213.
- [27] B. Moons, R. Uytterhoeven, W. Dehaene, and M. Verhelst, “14.5 en-vision: A 0.26-to-10tops/w subword-parallel dynamic-voltage-accuracy-frequency-scalable convolutional neural network processor in 28nm fdsoi,” in *2017 IEEE International Solid-State Circuits Conference (ISSCC)*. IEEE, 2017, pp. 246–247.
- [28] C. Farabet, B. Martini, B. Corda, P. Akselrod, E. Culurciello, and Y. LeCun, “Neuflo: A runtime reconfigurable dataflow processor for vision,” in *CVPR 2011 workshops*. IEEE, 2011, pp. 109–116.
- [29] Y.-H. Chen, T. Krishna, J. S. Emer, and V. Sze, “Eyeriss: An energy-efficient reconfigurable accelerator for deep convolutional neural networks,” *IEEE journal of solid-state circuits*, vol. 52, no. 1, pp. 127–138, 2016.
- [30] F. N. Iandola, S. Han, M. W. Moskewicz, K. Ashraf, W. J. Dally, and K. Keutzer, “Squeezenet: Alexnet-level accuracy with 50x fewer parameters and 0.5 mb model size,” *arXiv preprint arXiv:1602.07360*, 2016.